Bull. Chem. Soc. Ethiop. **2023**, 37(4), 1033-1045.
DOI: https://dx.doi.org/10.4314/bcse.v37i4.18

ISSN 1011-3924
Printed in Ethiopia
Online ISSN 1726-801X

GROWTH, CHARACTERIZATION AND CHEMICAL COMPUTATIONS OF GUANIDINIUM TRICHLOROACETATE (GTCA) SINGLE CRYSTAL – DFT APPROACH

R. Sreedevi[1*], A.S.I. Joy Sinthiya[2], T. Joselin Beaula[3], T. Balu[1] and P. Murugakoothan[4]

[1]Department of Physics, Aditanar College of Arts and Science, Tiruchendur, Tamil Nadu
[2]Department of Physics, The M.D.T. Hindu College, Tirunelveli, Tamil Nadu
[3]Department of Physics, Malankara Catholic College, Mariagiri, Tamil Nadu
[4]C. Kandaswamy Naidu College for Men, Chennai, Tamil Nadu

(Received July 21, 2022; Revised March 23, 2023; Accepted March 28, 2023)

ABSTRACT. Nonlinear optical (NLO) active guanidinium trichloroacetate (GTCA) crystal was synthesised and grown by using slow evaporation solution growth technique from mixed solvent. The grown crystal was characterized by single crystal X-ray diffraction (SXRD) and powder X-ray diffraction (PXRD) analysis. Fourier transform infrared (FTIR) spectrum of GTCA was recorded and the frequency assignments of various functional groups were compared with theoretical values. Mechanical strength of the grown crystal was studied using Vickers micro hardness tester. Thermal stability was studied using TG/DTA analyser. UV-Vis-NIR spectrum was recorded and the band gap energy was calculated. Geometry optimizations, first order hyperpolarizability, HOMO-LUMO energy gap, global reactive constants, thermodynamic properties, molecular electrostatic potential (MESP) and charge population were computed using B3LYP/6-31 G(d,p) basis set and DFT method and analysed.

KEY WORDS: PXRD, FTIR, TG-DTA, DFT, NBO, Charge population

INTRODUCTION

Nonlinear optics (NLO) is an emerging field which deals with the interaction of applied electromagnetic fields with materials to generate new electromagnetic fields, altered in wavenumber, phase or other physical properties [1]. Such a NLO material, capable of producing nonlinear signals have find applications in various fields like optical communication, signal processing, sensing optical computing and dynamic image processing etc. [2-4]. Organic materials are found to be more efficient candidate for NLO applications than inorganic and semi-organic counterpart due to their large nonlinear optical response [5, 6]. Recent reports highlight that guanidinium and its derivatives have been an organic potential candidate for NLO applications [7-10]. Since urea derivative guanidinium cation has broad family of hydrogen bond with delocalized conjugated π-electron leading to large NLO properties and quick response [11]. π-Electron conjugated system can enhance the required asymmetric distribution of electron in either the ground state or excited state. Design of such acentric materials, suggests that the hydrogen bonding network as the most remarkable methods in crystal engineering [12]. In the case of guanidinium complexes, the guanidinium cation has the ability of forming hydrogen bonded configurations with other electron donating groups [13].

Dipole present in the carboxylic groups enhances its ability to participate in the hydrogen bonding interactions with guanidinium cation. Hence recently an effort has been made in preparing acentric materials through hydrogen bonding using guanidinium carbonate and trichloroacetic acid by Dhavamurthy *et al.* [14]. As per authors knowledge no literature found regarding thermal, mechanical, spectral analysis and theoretical analysis with the aid of DFT computations. Hence, quantum chemical computations has been carried out with B3LYP/6-

*Corresponding author. E-mail: vsreedevi70@gmail.com

31G(d,p) basis set using Gaussian'09 software. The present work aims to investigate the spectral studies using FTIR spectrum, optical studies using UV-Vis-NIR spectrophotometer, mechanical studies using Vickers microhardness method, thermal studies using TG-DTA method. Structural, vibrational characterization, first order hyperpolarizability, molecular electrostatic potential (MESP), natural bond analysis (NBO), charge population, thermodynamic properties, HOMO-LUMO energy band gap have been performed using DFT computational method.

EXPERIMENTAL

Synthesis

The AR grade guanidinium carbonate and trichloroacetic acid was used for synthesizing the title salt. Guanidinium carbonate and trichloroacetic acid were taken in 1:1 molar ratio and dissolved in mixed solvent methanol and deionised water in 1:1 ratio and stirred well to get homogeneous mixture. The solution was filtered and allowed to evaporate and the synthesized salt was collected after 25 days. The purity of the synthesized salt was improved by repeated recrystallization. The synthesized salt was dissolved in 100 mL of mixed solvent and stirred well for 2 hours using magnetic stirrer to get saturated solution. Saturated solution was filtered using No. 1 grade Whatmann filter paper. The filtered solution was kept at room temperature. After 30 days needle shaped crystals of size 34×4×2 mm^3 were harvested. The photograph of one such grown crystal is shown in Figure 1(a).

Characterization

Grown GTCA crystal was characterized by single crystal X-ray diffraction analysis using Bruker Kappa APEX III diffractometer with MoKα radiation (λ = 0.71073 Å) to determine crystal structure. Powder X-ray diffraction (PXRD) spectrum was recorded in the 2θ range 20-80 degree using REICH SIEFERT X-ray diffractometer by employing CuKα radiation. Micro hardness analysis was carried out using LEITZ WETZLER Vickers microharness tester with diamond indenter. UV-Vis-NIR spectrum was recorded using Perkin Elmer Lamda 35 model spectrophotometer. TG-DTA analyses were carried out using Perkin Elmer Diamond thermal analyser in the nitrogen atmosphere and the thermo grams were recorded at the heating rate of 20 ºC/min from 40 ºC to 750 ºC.

Computational details

Quantum chemical analysis was performed at B3LYP/6-31G (d,p) basis set using Guassian'09 program. NBO calculations were performed using NBO 3.1 [15] program to understand inter and intra-molecular delocalization or hyperconjugation. Mulliken charge analysis and various thermodynamic functions were analysed. MESP, HOMO-LUMO energy gap and its related global constants, etc., were calculated. According to Koopman's theorem [16], the HOMO energy can be used to relate the ionization potential (IP) and the LUMO energy related to electron affinity (EA). Electronegativity (χ), electrophilicity index (ω), chemical hardness (η), global softness (S) and chemical potential (μ) were calculated [17]. First order hyperpolarizability β_{tot}, total static dipole moment (μ) and the polarizability (α) values [18] of GTCA were calculated using B3GLYP basis set, based on the finite field approach.

RESULTS AND DISCUSSION

Single crystal X-ray diffraction study

Grown GTCA crystal was subjected to single crystal X-ray diffraction study to determine crystal structure. Crystal system of GTCA is found to be tetragonal and the space group is $P4_3$. The

obtained unit cell parameters are a = b = 7.755 (9) Å, c = 15.523(3) Å and it is found to be in close agreement with the literature [14].

Powder X-ray diffraction analysis

Powder X-ray diffraction (PXRD) spectrum was recorded and pattern indexed using INDEX software is shown in Figure1b. The sharp peaks indicate the perfect crystalline nature of the grown crystal. The calculated cell parameters from the (h k l) values are a = b = 7.747 Å, c = 15.602 Å which is in good agreement with single crystal XRD data.

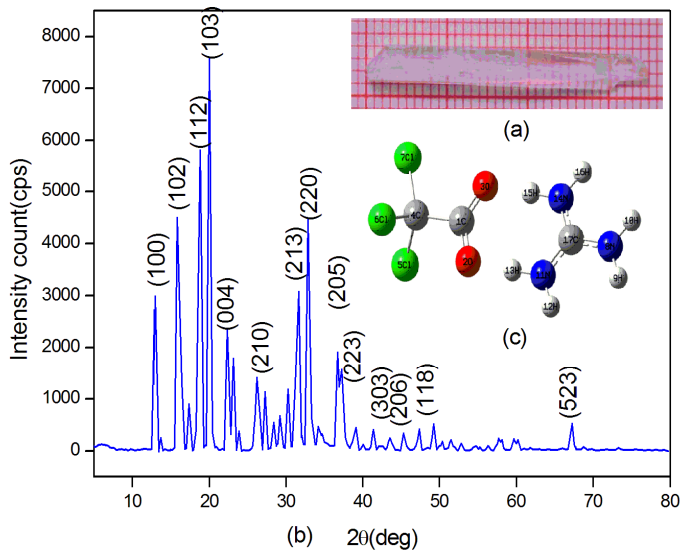

Figure 1. (a) Photograph of grown crystal, (b) PXRD pattern and (c) Molecular structure of GTCA crystal.

Geometrical structure

The structure data of GTCA was collected using single crystal diffraction technique. The structure of GTCA is found to be the same as that of the reported [14], though the solution used for synthesis was different. The experimental XRD data is used to get theoretical structure using Gaussian'09 software program package. Optimized structure of GTCA with atom labelled is shown in Figure 1(c) and optimized structural parameters calculated by DFT/B3LYP using 6-31G (d,p) basis set are listed in Table 1. In the case of GTCA, the inter-molecular interaction takes place between guanidinium cation and trichloro acetic anionic groups through N-H...O hydrogen bond. Guanidinium has three NH_2 groups, in which two of them are involved in intermolecular hydrogen bonding and hence any one of NH groups of these two amine show the elongation in the bond lengths than the others. N_{11}-H_{13} has the bond length as 1.0704 Å and N_{14}-H_{15} has 1.066 Å. DFT indicates the presence of intermolecular N-H...O hydrogen bond for GTCA as it is evident from the O-H bond lengths O_2-H_{13} (1.565 Å) and O_3-H_{15} (1.586 Å). The bond angles C_{17}-N_{14}-H_{15}, C_{17}-N_{11}-H_{13} in the perturbed NH_2 of guanidine group shows the vibrant variation than the other

unperturbed NH_2 which may be involved in moderate hydrogen bonding. These predicted bond angles and bond lengths show the intermolecular hydrogen bonding interaction between the guanidine and the acid group and are comparable with experimental data.

Table 1. Optimized structural data.

Bond length	Theo. (Å)	Exp. (Å)	Bond angle	Theo. (°)	Exp. (°)
C_1-O_2	1.252	1.21(2)	O_2- C_1-O_3	129.736	126.7(11)
C_1-O_3	1.249	1.27(2)	O_2-C_1-C_4	113.809	118.4(16)
C_1-C_4	1.585	1.496(17)	O_3-C_1-C_4	116.456	114.8(15)
C_4-Cl_5	1.806	1.633(15)	C_1-C_4-Cl_5	108.568	104.5(11)
C_4-Cl_6	1.806	1.671(16)	C_1-C_4-Cl_6	108.562	104.2(10)
C_4-Cl_7	1.792	1.762(14)	C_1-C_4-Cl_7	112.678	114.9(12)
N_8-H_9	1.006	0.860	Cl_5-C_4-Cl_6	109.191	107.1(10)
C_{17}-N_8	1.359	1.326(3)	Cl_5-C_4-Cl_7	108.896	101.5(10)
N_{11}-H_{12}	1.007	0.860	Cl_6-C_4-Cl_7	108.896	110.0(10)
N_{11}-H_{13}	1.070	0.860	H_9-N_8-$C1_7$	121.081	120.02
C_{17}-N_{11}	1.327	1.228(19)	H_{10}-N_8-$C1_7$	121.126	120.03
N_{14}-H_{15}	1.066	0.860	H_{12}-N_{11}-H_{13}	119.654	120.0
N_{14}-H_{16}	1.007	0.860	H_{12}-N_{11}-C_{17}	119.771	120.0
N_{14}-C_{17}	1.328	1.409(19)	H_{13}-N_{11}-C_{17}	120.576	120.0
O_2-H_{13}	1.565	2.00	H_{15}-N_{14}-H_{16}	119.574	120.0
O_3-H_{15}	1.586	2.07	H_{15}-N_{14}-C_{17}	120.562	120.0
			H_{16}-N_{14}-C_{17}	119.865	120.0
			N_8-C_{17}-N_{11}	120.057	127.1(15)
			N_8-C_{17}-N_{14}	119.914	112.6(15)
			N_{11}-C_{17}-N_{14}	120.029	120.3(11)
			N_{11}-H_{13}-O_2	-	169.5
			N_{11}-H_{15}-O_3	-	164.0

NBO analysis

The values obtained in NBO analysis are presented in Table 2 was used to elucidate inter and intra molecular hydrogen bonding, intermolecular charge transfer. Lone pair interactions between Guanidinium moiety to trichloroacetate moiety n1(O_2)→ σ*(N_{11}-H_{13}), n2(O_2)→ σ*(N_{11}-H_{13}), n2(O_3)→ σ*(N_{14}-H_{15}) and n2(O_3)→ σ*(N_{14}-H_{15}) obtained as 10.62, 41.61, 38.77 and 9.82 kcal/mol, respectively serves as an evidence for charge transfer interactions from Guanidinium moiety to trichloroacetate moiety. Interaction between the lone-pair n2(O_2) and n2(O_3) with the antibonding orbital N_{11}-H_{13} … O_2 and N_{14}-H_{15} …O_3 reveals the presence of N-H…O intermolecular hydrogen bonding. Lone pair of n3(O_2) with π*(C_1-O_3) is identified as the strongest (114.94 kcal/mol) interaction.

Table 2. Second order perturbation theory analysis of Fock matrix in NBO basis.

Donor (i)	ED(i) (e)	Acceptor (j)	ED (j) (e)	[a]E(2) (kcalmol^{-1})	[b]E(j)-E(i) (a.u.)	[c]F(i,j) (a.u.)
n1(O_2)	1.95280	σ*(N_{11}-H_{13})	0.10585	10.62	1.04	0.095
n2(O_2)	1.81145	σ*(N_{11}-H_{13})	0.10585	41.61	0.75	0.161
n2(O_3)	1.81668	σ*(N_{14}-H_{15})	0.10097	38.77	0.75	0.155
n1(O_3)	1.95459	σ*(N_{14}-H_{15})	0.10097	9.82	1.05	0.092
n3(O_2)	1.61248	π*(C_1-O_3)	0.39978	114.94	0.25	0.151

[a]E(2) = means energy of hyper conjugative interactions. [b]E(j)-E(i) = energy difference between donor and acceptor i and j NBO orbitals. [c]F(i,j) is the Fockmatrix element between i and j NBO orbitals.

FT-IR analysis

FT-IR spectrum was recorded in the region 4000 cm^{-1} to 400 cm^{-1}. The observed frequencies with TED contributions are listed in Table 3.

Table 3. Vibrational assignment of GTCA.

Unscaled wavenumber (cm^{-1})	Scaled wavenumber (cm^{-1})	Experimental wavenumber (cm^{-1}) IR	Assignments with (TED%) VEDA
3768.19	3632.535	-	νN_8-H_9 (50), νN_8-H_{10} (50)
3685.896	3553.204	-	νN_{14}-H_{16} (86), νN_{11}-H_{12} (13),
3682.524	3549.953	3381	νN_{11}-H_{12} (86), νN_{14}-H_{16} (13)
3643.392	3512.23	3157	νN_8-H_9 (50), νN_8-H_{10} (50)
2720.516	2622.577	2820	νN_{14}-H_{15} (64),νN_{11}-H_{13} (29),
2541.162	2449.68	-	ν N_{11}-H_{13} (60), νN_{14}-H_{15} (30),
1774.455	1710.575	1662	νC_2-O_1(10), νC_1-O_3 (12), νN_{11}-C_{17} (22), νN_{14}-C_{17} (20), βH_{15}-N_{14}-C_{17}(10),
1753.642	1690.511	-	βH_{12}-N_{11}-H_{13}(28), βH_{16}-N_{14}-H_{15}(26), βH_{15}-N_{14}-C_{17}(18), βC_{17}-N_{11}-H_{13}(13),
1728.685	1666.452	-	ν C_2-O_1 (27), ν C_1-O_3 (27), βH_{12}-N_{11}-H_{13}(11), βH_{16}-N_{14}-H_{15}(11),
1683.364	1622.763	-	βH_9-N_8-H_{10}(55),νN_8-C_{17} (21),
1598.156	1540.622	1574	βH_9-N_8-H_{10}(36),νN_{11}-C_{17} (18), νN_{14}-C_{17} (16),
1591.243	1533.958	1418	νN_{14}-C_{17} (26), βH_{12}-N_{11}-H_{13}(16),
1386.269	1336.363	1338	ν C_2-O_1 (44), ν C_1-O_3 (41),
1165.532	1123.573	1152	βH_{15}-N_{14}-C_{17}(29), βH_{16}-N_{14}-H_{15}(14), βH_9-N_8-C_{17}(12), βH_{12}-N_{11}-H_{13}(11),βO_3-C_1-O_2(10),
1161.692	1119.871	-	βH_{12}-N_{11}-H_{13}(19), βH_{12}-N_{11}-H_{13}(18), βH_{15}-N_{14}-C_{17}(17), νN_{14}-C_{17} (14), βH_{16}-N_{14}-H_{15}(14),
1060.679	1022.495	-	βH_9-N_8-C_{17}(69),
1028.45	991.4258	1110	νN_{14}-C_{17} (43),νN_{11}-C_{17} (25), νN_{14}-C_{17} (27),
1022.727	985.9088	-	τO_2-H_{13}-N_{11}-C_{17}(28), τH_{12}-N_{11}-H_{13}-O_2(25), τC_1-O_3-H_{15}-N_{14}(18), τH_{16}-N_{14}-H_{15}-O_3(17),
960.8367	926.2466	938	τH_{16}-N_{14}-H_{15}-O_3(39), τC_1-O_3-H_{15}-N_{14}(25),τH_{12}-N_{11}-H_{13}-O_2(18),
938.1846	904.41		νC_4-C_1(53, βO_3-C_1-O_2(12),
831.7275	801.7853	841	τC_4-O_3-O_2-C_1(59), τCl_7-C_1-Cl_6-C_4(16),
811.6027	782.385	-	νCl_7-C_4(32), βC_4-C_1-O_2(19), τCl_6-C_1-Cl_5-C_4(15), τCl_7-C_1-Cl_6-C_4(12),
754.2096	727.0581	750	βO_3-C_1-O_2(64),
718.5934	692.724	681	τN_8-N_{11}-N_{14}-C_{17}(76),
657.8444	634.162	607	νCl_5-C_4(30), νCl_6-C_4(30),
588.8022	567.6053	527	βN_{14}-C_{17}-N_{11}(76),

Guanidinium vibrations

NH_2 group asymmetric and symmetric stretching vibrations [19] give rise to a strong bands in the region 3390 ± 60 cm^{-1} and 3210 ± 60 cm^{-1} respectively. In GTCA molecule the scaled value at 3550 cm^{-1} is assigned to the asymmetric stretching vibration NH_2 which is observed in IR at 3381 cm^{-1} (strong) and the scaled value at 3512 cm^{-1} is assigned to the symmetric stretching vibration of NH_2 which is observed in IR at 3157 cm^{-1} (strong). NH_2 scissoring vibrations give rise to a band in the region 1620 ± 20 cm^{-1} and rocking vibration in the range 1195 ± 90 cm^{-1} [19]. These bending vibrations modes are observed and presented in Table 3.

Guanidinium compound absorb strongly at 1685-1580 cm^{-1} due to C-N stretching vibrations [20], which is observed as a very strong band in IR at 1574 cm^{-1}. It has been reported that C-N stretching of aliphatic amine compounds is generally weak and occurs in the region of 1220-1020 cm^{-1} [21] which is observed in IR at 1110 cm^{-1}. Medium to weak intensity bands in the frequency range 600-400 cm^{-1} are due to CNC deformation vibrations [22] which is observed in IR as a strong band at 527 cm^{-1}.

Chloroacetate vibrations

Vibration belonging to the link between the C–Cl is significant to discuss here since mixing of vibrations are possible due to the lowering of the molecular symmetry and the presence of heavy atoms on the periphery of the molecule [23]. C–Cl stretching vibration gives generally a strong band in the region 750–580 cm^{-1} [24-26] which is observed in IR as a strong band at 607 cm^{-1}

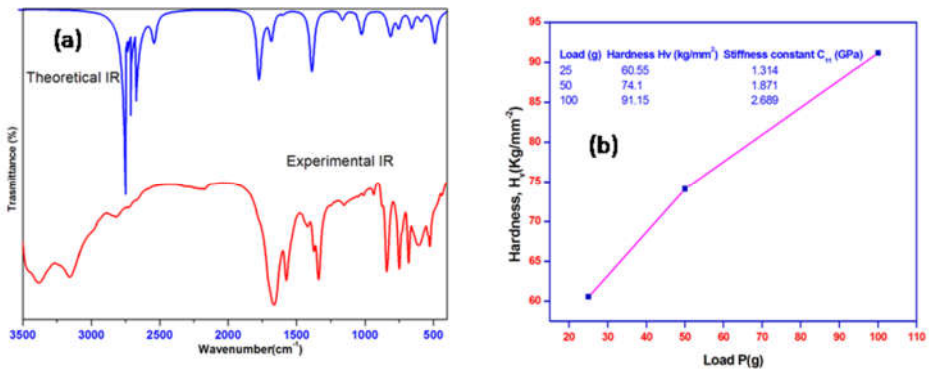

Figure 2. (a) FTIR spectrum and (b) Hardness vs load plot with stiffness constant of GTCA.

Asymmetric and symmetric stretching modes of carboxylate ion vibrations expected to occur in the range 1650-1550 cm^{-1} and near 1440 cm^{-1}, respectively [27]. Asymmetric stretching of COO^- vibration appears in IR at 1662 cm^{-1} as a strong band and symmetric stretching band is observed at 1338 cm^{-1} in IR. Unusual lowering of the carboxylate asymmetric stretching wavenumber is contributed by the electron releasing effect of the CO bond in the acceptor subunit due to intermolecular charge transfer effect and conjugation effect which plays an important role in the NLO activity of GTCA. The acid group COO^- deformations are usually expected to occur in the region 760–400 cm^{-1} [22, 27]. COO^- bending mode appears as a very strong band at 750 cm^{-1} in IR which is in good agreement with the theoretical value. All the frequency assignments are compared with the experimental data and the theoretical and experimental graphs, are shown in Figure 2(a), explore the evidence for the GTCA structural formation.

Microhardness analysis

It is essential to study the mechanical properties to avoid loss of material during device fabrication [28]. Hence Vickers hardness test was carried out for various loads ranging from 25-100 g and the hardness nature GTCA crystal is depicted in Figure 2(b). The linearity of hardness with load represents the need of high stress beyond 100 g to generate dislocation and crack by indentation. It shows the highly impressive elastic nature and is validated from the stiffness constant data

presented in Figure 2(b). High stiffness constant shows the strong binding force between the molecules of GTCA compound which explored the good mechanical strength and hence applicable in the laser based devices.

UV-Vis-NIR spectral analysis

UV-Vis-NIR spectrum of grown GTCA crystal was recorded from 190-1100 nm and the spectra is shown in Figure3a. It is clear from the spectrum that there is no absorption observed above 255 nm and has 40% transmittance. Compared to the reported value [14], the lower cut-off wavelength is low but has lower percentage of transmittance which attributes the solvent effect. The optical band gap has been calculated [29], from the extrapolation of the linear part of Tauc's plot, as shown in Figure 3b, and is found to be 4.56 eV. The transparency in the entire visible region confirms the suitability of the material for opto-electronic device fabrication.

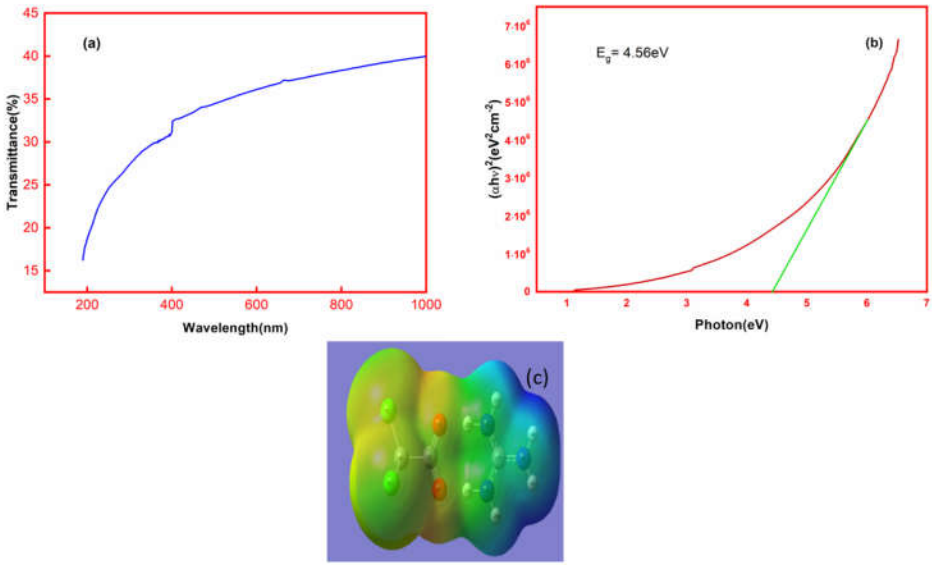

Figure 3. (a) UV-Vis-NIR spectrum, (b) Tauc's plot and (c) MESP diagram of GTCA crystal.

Molecular electrostatic potential diagram

Molecular electrostatic potential (MESP) plot is a useful descriptor for the qualitative interpretation of the electrophilic and nucleophilic sites and hydrogen bonding interactions [30] and MESP plot of GTCA is shown in Figure 3(c). MESP map displays the positive, negative and neutral centres in terms of colour grading. The deep red colour which are located over carboxylic acid group represents electrophilic centres and the deep blue colour regions located over guanidinium represents nucleophilic centres. These are due to transfer of charge from electron rich trichloroacetic acid to guanidinium group. This observation confirms the existence of the two reactive regions, and hence hydrogen bonding interaction, which ensures the active optical properties of GTCA compound making it a suitable NLO active material.

Frontier molecular orbital analysis

Frontier molecular orbital (HOMO-LUMO) analysis was performed at DFT/B3LYP level to explain the electronic and optical properties as well as chemical reactions [31]. Figure 4(a) illustrates the frontier molecular orbital transitions for GTCA. HOMO-LUMO plot explains the nature of reactivity and some of the structural and physical properties of molecules.

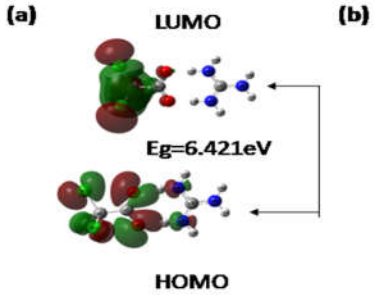

Parameters	B3LYP/6-31G(d,p)
HOMO energy (eV)	-6.6774
LUMO energy (eV)	-0.2561
HOMO-LUMO energy gap (eV)	6.42eV
Ionization potential, IP (eV)	6.6774
Electron affinity, EA (eV)	0.2561
Electronegativity,χ (eV)	3.4667
Chemical hardness,η (eV)	3.2107
Global softness, S (eV^{-1})	0.1557
Chemical potential, μ (eV)	-3.4667
Electrophilicity index, ω (eV)	1.8716

Figure 4. (a)HOMO-LUMO Plot (b) Global constants of GTCA.

Energy gap between HOMO and LUMO reflects the kinetic stability, chemical reactivity, molecular polarizability, softness and hardness of the molecules. A molecule with smaller frontier molecular orbitals is associated with high chemical reactivity, low kinetic stability and more intermolecular interactions due to which the molecule is termed as soft molecule and large value of HOMO-LUMO energy gap indicates the chemical hardness. The calculated values of global descriptors are presented in the table given in Figure 4(b). HOMO-LUMO energy gap in the gaseous phase is found to be 6.421 eV which is greater compared to the combined molecules in the solid phase value 4.5 eV. This difference implies that the band gap in solid state is determined by the periodic, crystalline atomic structure of the material. Softness value is 0.1557 eV^{-1} and hardness value is 3.2107 eV. Thus the grown crystal has been predicted as a chemically stable material.

Thermal analysis

TG-DTA analyses were carried out and the thermograms are presented in Fig. 5(a). From the thermogravimetry analysis, it is observed that weight loss takes place between 195ºC and 300ºC with the weight loss of 59%. In step wise various gaseous fragments are eliminated and the residue left out at the end is about 9%. DTA curve shows, the endothermic transition at 195ºC, which in association with the weight loss, implies the decomposition of the sample. The heat energy absorbed at this temperature is utilised for the breaking of bonds during decomposition. The sharpness of the endothermic peak shows the good degree of crystallinity and purity of the material. Material shows the endothermic peak at 292 ºC and 448 ºC which corresponds to the stepwise decomposition of the compound.

Thermodynamic properties

Temperature dependent thermodynamic properties are the important parameter to study the reliable relations between structural, reactivity and energetic characterization of the grown crystal. Using DFT various statistical thermodynamic properties of the molecules were predicted. The thermodynamic parameter values of the title compound GTCA were calculated by B3LYP-6-31G(d,p) at 298.15 K and 1 atm pressure which are listed in table given in Figure 5(b). All theoretical values of enthalpy is found to be greater than zero and is clear evidence from the endothermic peak in experimental thermal analysis which shows the absorption of heat energy for bond dissociation. Thermodynamic parameters such as entropy, enthalpy and heat capacity for various temperature ranges from 100-1000 K is plotted in Figure 5(c). The plot shows the increase of all the parameters with the increase of temperature since the vibrational intensities of the molecules increases with temperature [32]. This behaviour attributed to the highly reactive nature of the title compound.

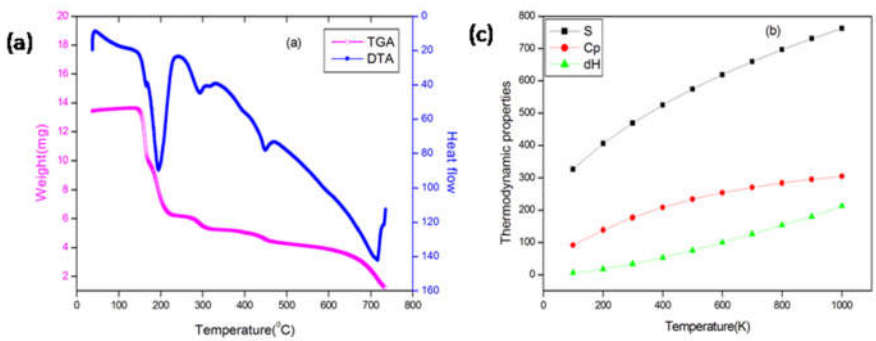

(b)

T (K)	$C^{0}_{p,m}$ ($Jmol^{-1}K^{-1}$)	AS^{0}_{m} ($Jmol^{-1}K^{-1}$)	AH^{0}_{m} ($kJmol^{-1}$)	AG=AH-TAS ($kJ\ mol^{-1}$)
100	92.08	327.19	6.21	-26.49
200	138.85	405.90	17.89	-63.29
298	176.87	468.66	33.45	-106.21
300	177.52	469.76	33.77	-107.16
400	209.04	497.35	53.16	-145.78
500	234.34	574.78	75.37	-212.02
600	254.61	619.36	99.86	-271.76
700	271.04	659.88	126.17	-335.75
800	284.57	696.99	153.97	-403.62
900	295.90	731.18	180.01	-478.05
1000	305.51	762.87	213.09	-549.78

Figure 5. (a) TG-DTA thermograms, (b) thermodynamic parameters of GTCA and (c) variation of thermodynamic parameters with temperature.

First order hyperpolarizability

Hyperpolarizability and NLO properties of an isolated molecule of potential NLO materials are considered as an extensive tool of research in molecular spectroscopy. First order hyperpolarizability, β_{tot} of the title compound GTCA was calculated using B3GLYP basis set, based on the finite field approach. The hyperpolarizability, polarizability and dipole moment values are given in Table 4. It is observed that the dipole moment and polaizability value are other

than zero which is the origin of the developing NLO property in the solid phase. First order hyperpolarizability is 3.4 times that of standard KDP [10] in the gaseous phase is validated for better the hyperpolarizabilty in the solid state of the GTCA compound.

Table 4. Hyperpolarzability (a.u.) for the title compound.

Dipole moment (Debye)	Values	Hyper-polarizability (a.u.)	Values	Polarizability	Values (a.u.)
μ_x	-4.80055	β_{xxx}	-226.2788	α_{xx}	112.0583
μ_y	0.02249	β_{xxy}	23.8711	α_{xy}	1.0239
μ_z	-0.00006	β_{xyy}	-64.0852	α_{yy}	96.0119
μ_{tot}	4.80 Debye	β_{yyy}	-11.4151	α_{xz}	0.0091
		β_{xxz}	-0.0204	α_{yz}	0.0006
		β_{xyz}	-0.0252	α_{zz}	65.6262
		β_{yyz}	-0.0095		
		β_{xzz}	14.3920		
		β_{yzz}	0.8342	α_{tot}	13.52×10^{-24} esu
		β_{zzz}	-0.0103		
		β_{tot}	23.124×10^{31} esu		

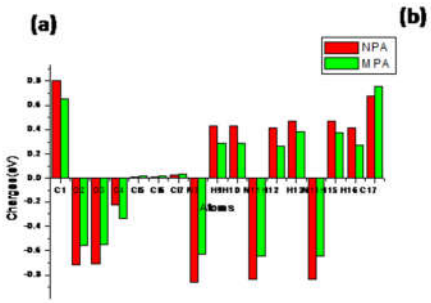

Atom	NPA Charge	Mulliken Charge
C_1	0.80422	0.650109
O_2	-0.71687	-0.557213
O_3	-0.70647	-0.551318
C_4	-0.22324	-0.336492
Cl_5	0.01485	0.019072
Cl_6	0.01486	0.019076
Cl_7	0.02884	0.037026
N_8	-0.85521	-0.630467
H_9	0.43086	0.290242
H_{10}	0.43066	0.290039
N_{11}	-0.83255	-0.643372
H_{12}	0.41629	0.268764
H_{13}	0.46900	0.384359
N_{14}	-0.83347	-0.642675
H_{15}	0.46807	0.378912
H_{16}	0.41653	0.269257
C_{17}	0.67363	0.754682

Figure 6. (a) Charge population plot and (b) NPA and MPA charge distribution of GTCA.

Charge analysis

Analysis of effective atomic charges plays a vital role in the application of quantum chemical calculations to molecular system. Calculated natural atomic charge values from the natural population analysis (NPA) and Mulliken charge analysis procedures using DFT methods are listed in the table given in Figure 6(b) and the comparative graph is given in Figure 6(a).

Charge on hydrogen atoms H_{13} and H_{15} involves in intermolecular hydrogen bonding which is more positive than the other hydrogen atoms. The charges on carboxylic carbon atom C_1 and guanidinium group carbon C_{17} are positive while trichloro carbon C_4 is negative which is due to electron donating natures of oxygen and electron withdrawing nature chlorine and nitrogen. This result confirms the redistribution of electron density due to substitution effect. Thus Mulliken

charge analysis and natural population analysis of GTCA quantify how the electronic structure changes under atomic displacements. It is therefore related directly to chemical bonding.

CONCLUSION

GTCA crystal was grown and characterized. The single crystal X-ray diffraction analysis shows the crystal belongs to tetragonal structure with space group $P4_3$. Powder X-ray diffraction (PXRD) diffraction study reveals the perfect crystalline nature of the grown crystal. The experimental and theoretical FTIR spectral analysis was compared. The various functional groups present in GTCA compound were confirmed. UV-Vis-NIR optical study reveals the linear optical nature of the title compound without any absorption in the entire visible region. Vickers microharness analysis reveals the strength of the material. Optimized geometrical parameters were calculated, which confirms the formation of GTCA compound through hydrogen bonding. The quantum chemical analysis using DFT calculations were carried out and various electronic properties were analysed. HOMO-LUMO energy gap and its tailoring global constants were calculated. All the calculated values of global constants show the soft chemical nature of title compound. NBO analysis confirms the nature of bonding between the two reactants in the GTCA compound. The thermodynamic properties show the chemical reactivity of the molecules. MESP plot suggests the charge transfer nature of the molecules. NPA and MPA analysis shows the donor and acceptor sites and its charge density between the guanidinium moiety and trichloroacetate moiety.

ACKNOWLEDGEMENTS

One of the authors (R. Sreedevi) is grateful to the management of Aditanar College of Arts and Science, Tiruchendur for the encouragement given to her to carry out the research work. This work is partially supported by University Grants Commission (UGC), Government of India, under UGC-SAP-Basic Science Research Program. The author would like to thank Mahatma Gandhi University, Kottayam for providing SXRD characterization facility.

REFERENCES

1. Shen, Y.R. *The Principles of Nonlinear Optics*, Wiley: New York; **1984**.
2. Kolinsky, P.V. New materials and their characterization for photonic device applications. *Opt. Eng.* **1992**, 31, 1676-1685.
3. Eaton, D.F. Nonlinear optical materials. *Science* **1991**, 253, 281-287.
4. Ramasamy, G.; Meenakshisundaram, S. Studies on amino acid picrates: Crystal growth, structure and characterization of new non-linear optical material L-isoleucinium picrate. *Optik* **2014**, 125, 4422-4426.
5. Pal, T.; Kar, T.; Bocelli, G.; Rigi, L. Synthesis, growth and characterization of L-arginine acetate crystal: A potential NLO material. *Cryst. Growth Des.* **2003**, 3, 13-16.
6. Gu, B.; Wang, Y.H.; Peng, X.C.; Ding, J.P.; He, J.I.; Wang, H.T. Giant optical nonlinearity of a $Bi_2Nd_2Ti_3O_{12}$ ferroelectric thin films. *Appl. Phys. Lett.* **2004**, 85, 3687-3689.
7. Saravanakumar, G.; Manobalaji, G.; Murugakoothan, P. Experimental and theoretical Investigations on N-N'-diphenyl phosphate - A semi-organic nonlinear optical material. *Spectrochim. Acta Part A: Mol. Biomol. Spectrosc.* **2015**, 138, 340-347.
8. Suvitha, A.; Sathyanarayanamoorthy, V.; Murugakoothan, P. Growth, spectroscopy properties and DFT based DCM calculations of guanidinium chlorochromate. *Spectrochim. Acta Part A, Mol. Biomol. Spectrosc.* **2013**, 110, 255-261.

9. Sasikala, V.; Sajan, D.; Job Sabu, K.; Arumanayagam, T.; Murugakoothan, P. Electronic structure, vibrational, spectral and intervening orbital interactions studies of NLO materials guanidinium 4-nitrobenzoate. *Spectrochim. Acta Part A: Mol. Biomol. Spectrosc.* **2015**, 139, 555-572.
10. Saravanakumar, G.; Vivek, P.; Murugakoothan, P. A combined experimental and quantum chemical analysis to explore the nonlinear optical activity of guanidinium L-mono hydrogen tartrate. *Spectrochim. Acta Part A: Mol. Biomol. Spectrosc.* **2015**, 145, 417-424.
11. Sivashankar, V.; Siddhesswaran R.; Murugakoothan, P. Synthesis, growth, structural, optical and thermal properties of a new semiorganic nonlinear optical guanidinium perchlorate single crystal. *Mater. Chem. Phys.* **2011**, 130, 323-326.
12. Guru Row, T.N. Hydrogen and fluorine in crystal engineering systematic from crystallographic studies of hydrogen bonded tartrate – amine complexes and fluorosubstituted coumarines, styryl coumarine and butadienes. *Coord. Chem. Rev.* **1999**, 183, 81-100.
13. Dhanraj, P.V.; Rajesh, N.P. Vinitha G.; Bhagavannarayana, G. Crystal structure and characterization of a novel organic optical crystal: 2-Aminopyridinium trichloroacetate. *Mater. Res. Bull.* **2011**, 46, 726-731.
14. Dhavamoorthy, M.; Peramaiyan, G.; Nizam Mohideen, M.; Kalainathan, S.; Mohan, R. Structural, growth and optical characterization of an organic third order nonlinear crystal: Guanidinium trichloroacetate. *J. Nonlinear Opt. Phys. Mater.* **2015**, 24, 1550045.
15. Glendening, E.D.; Reed, A.E.; Carpenter, J.E.; Weinhold, F. *NBO Version3.1*, Theoretical Chemistry Institute and Department of Chemistry, University of Wisconsin, Madison; **1998**.
16. Koopman, T.A. Ordening of wavefunctions and eigen energies to the individual electrons of an atom. *Physica B* **1993**, 1, 104-113.
17. Sasikala, V.; Sajan, D.; Job Sabu, K.; Arumanayagam, T.; Murugakoothan, P. Electronic structure, vibrational spectral and intervening orbital interactions studies of NLO material: Guanidinium 4-nitrobenzoate. *Spectrochim. Acta Part A: Mol. Biomol. Spectrosc.* **2015**, 139, 555-572.
18. Kleinman, D.A. Nonlinear dielectric polarization in optical material. *Phys. Rev.* **1962**, 126, 1977-1979.
19. *Interpretation of Infrared Spectra, A Practical Approach by John Coates in Encyclopedia of Analytical Chemistry*, John Wiley and Sons: Chichester; **2000**; pp. 10815-10837.
20. Socrates, G. *Infrared and Raman Characteristic Group Frequencies, Tables and Charts*, 2nd ed., Wiley: New York; pp. 341-342, **2001**.
21. Colthup, N.B.; Daly, L.H.; Wiberly, S.E. *Introduction to Infrared and Raman Spectroscopy*, 3rd ed., Academic Press: New York; **1990**; pp. 258-275.
22. Dollish, F.R.; Fateley, W.G.; Bentley, F.F. *Characteristic Raman Frequencies of Organic Compounds*, John Wiley and Sons: New York; **1997**; pp. 135-137, 162-190, 263-272.
23. Lee, C.; Yang, W.; Parr, R.G. Development of Colle-Salvetti correlation-energy formula in to a functional of the electron density. *Phys. Rev. B* **1988**, 37, 785-789.
24. Hiremath, C.S. Sundius, T. Vibrational spectra, abinitio/DFT electronic structure calculations and normal co-ordinate analysis of 2-bromo-5-fluorobenzaldehyde. *Spectrochim. Acta A* **2009**, 74, 1260-1266.
25. Mooney, E.E. The infrared spectra of chloro and bromobenzene derivatives -1: Anisoles and phenetoles. *Spectrochim. Acta A* **1968**, 19, 877-881.
26. Mooney, E.E. The infrared spectra of chloro and bromobenzene derivatives II: nitrobenzoate. *Spectrochim. Acta A* **1964**, 20, 1021-1024.
27. Socrates, *G. Infrared and Raman Characteristic Group Frequencies*, 3rd ed., John Wiley and Sons: England; **2001**; pp. 128-129.
28. Anciya, S.; Joy Sinthiya, A.S.I.; Selvarajan, P.; Sree Devi, R. Imidazole added sulphamic acid single crystals with optimal properties for optoelectric devices. *Mater. Today Proceed.* **2022**, 49, 2276-2282.

29. Vivek, P.; Murugakoothan, P. Second and third order optical studies of 4-bromoanilinium hydrogen phthalate single crystal for nonlinear optical device applications. *Appl. Phys. A* **2014**, 115, 1139-1146.
30. Lukue, F.J.; Lopez, J.M.; Orozco, M. Perspective on electrostatic interactions of a solute with a continuum. A direct utilization of abinitio molecular potentials for the precision of solvent effects. *Ther. Chem. Acc.* **2000**, 103, 343-345.
31. Parlak, C.; Akdogan, M.; Yildinm, G.; Karagoz, N.; Budak, E.; Terzioglu, C. Density functional theory study on the identification of 3[(2-morpholinoethlimine)methyl] benzene-1,2 diol. *Spectrochim. Acta Part A* **2011**, 79, 263-271.
32. Ceylan, U.; Gonca Ozdemit, T.; Halil, G.; Erbil, A. Spectroscopic (FTIR and UV-Vis) and theoretical (HF-DFT) investigations of 2-ethyl-N-[5-nitrothiophane-2yl)methylidene] aniline. *J. Mol. Struc.* **2016**, 1110, 1-10.